Geophys. J. Int. (1989) **98,** 69–84

An inverse approach to heat flow study in hydrologically active areas

K. Wang and A. E. Beck

Department of Geophysics, University of Western Ontario, London, Ontario, Canada N6G 5B7

Accepted 1988 December 21. Received 1988 October 9; in original form 1988 June 6.

SUMMARY

Heat transport by large-scale groundwater movement, reported for a number of sedimentary basins, may cause sufficiently severe perturbations to the thermal regime that the patterns of near surface heat-flow density (HFD) may be very different from that of the desired deep-seated conductive HFD. However, a good interpretation of the HFD data from perturbed areas is possible when knowledge of both the thermal and hydrological regimes is available, but there are three major difficulties. First, the thermal and hydrological data are often noisy; second, the two regimes are closely coupled; third, the deep-seated, or basal HFD is a very uncertain boundary condition. In this paper, we present a method, currently in 2-D, that inverts the noisy thermal and hydrological data simultaneously, and is able to resolve uncertain boundary conditions. The temperature and hydraulic head and the thermal conductivities and intrinsic permeabilities of the subsurface materials are first parameterized with an isoparametric finite element model. The parameters are then estimated using a Bayesian type non-linear inverse method. In the finite element formulation, the boundary heat and water fluxes are linearly transformed into an equivalent nodal flow (ENF) vector, which is updated together with the estimated parameters. Another (linear) inversion of the updated ENF components gives the updated boundary fluxes, with variances. The applications of the boundary flux updating technique to the determination of the background HFD in hydrologically active areas are illustrated with numerical examples.

Key words: coupled geothermal–hydrological problem, finite element, general inverse method, heat flow density, hydrology

INTRODUCTION

Hydrodynamic contributions to the geothermal regime have long been of concern to terrestrial heat-flow researchers, but it was usual to assume that the effects on the conductive thermal regime were not significant if there were no obvious warning signatures in the temperature–depth plots (such as significant curvature in temperature gradients). However, in recent years it has become more evident that this criterion is not valid and that gravitationally driven groundwater movements may give rise to regional scale advective heat transfer to disturb substantially, and perhaps control, the subsurface temperature field; therefore the HFD values determined from near surface measurements may be unrepresentative of the conductive regime. For example, Majorowitz & Jessop (1981) and Jones, Majorowitz & Lau (1985) analysed bottom hole temperature (BHT) data, thermal conductivity and preCambrian basement rock heat generation of the western Canada sedimentary basin and concluded that groundwater flow is the most plausible reason for the observed uneven surface HFD pattern of low values in the SE, where groundwater recharge takes place, and high values in the NW, where groundwater discharge takes place. Their conclusion was supported by the study of the overall groundwater flow pattern of the basin (Hitchon 1984). A number of other similar cases can be found in the literature, e.g. Chapman *et al.* (1984), Čermak & Jetel (1985), Wang *et al.* (1985), Gosnold & Fischer (1986), Willet & Chapman (1987) and Čermak (1989). Numerical modelling of the interaction between the thermal and hydrological regimes of basin scale has also been performed by, for example, Mercer, Pinder & Donaldson (1975), Smith & Chapman (1983), Bethke (1985), Wang *et al.* (1985), Luheshi & Jackson (1986) and Willet & Chapman (1987) using 2-D models and Woodbury & Smith (1985) using a 3-D model.

These studies on the interaction between the hydrological and thermal regimes have resulted in very useful databases and, though some interpretations are largely qualitative and some conclusions subject to debate (Bachu 1985), much insight into the problem has been gained. However, the determination of the basal conductive HFD, the thermal signal from the deeper part of the Earth's crust, is still a problem in hydrologically active regions, that is, in regions where the groundwater flow is strong enough to give significant thermal effects. When forward numerical modelling techniques are used, the basal HFD, as a Neumann-type boundary condition, has to be estimated on a trial-and-error basis. In addition, thermal and hydrological data may be very noisy in the sense that they contain large errors, hence a quantitative method that can optimally utilize all the available information is needed. Inverse

theories, which incorporate relevant physical laws and statistical principles, are default candidates for such a method. Since the quality and sufficiency of thermal and hydrological data vary greatly, the parameters to be resolved by an inverse method may vary from problem to problem. For example, there may be very accurate measurements on the field variables, such as temperature (T) and hydraulic heat (h), in a portion of a study area where the values for the material properties, thermal conductivity (λ) and permeability (κ), are lacking; at the same time, in another portion of the same area, the material properties may be well known but the field variables poorly determined. When boundary conditions are very uncertain or even unknown, the situation is even more complicated. Therefore, an inverse method of system identification, which uses field variable data to identify material properties (or system parameters), is too limited for our problem. This paper is intended to present a generalized inverse method that, in addition to being computationally efficient, has the following basic characteristics:

(1) The thermal and hydrological data can be inverted simultaneously, as in Kasameyer *et al.* (1985) and Woodbury & Smith (1988), so that the information contained in the data on the interaction of the two regimes can be used quantitatively.

(2) The material properties and field variables are formulated equally as parameters, an approach recommended by Tarantola & Valette (1982). With this approach, better use is made of the total amount of information rather than relying on the availability of good information on one or two specific physical quantities. For example, inadequate knowledge of boundary conditions can be compensated by better knowledge of field variables and material properties; poor quality field-variable data can be compensated by good quality material property data; and so on.

(3) It can provide the best estimate of the basal HFD values. When the basal HFD is to be determined by an inverse method, the common practice is to form the problem in such a way that the HFD is one of the parameters (Vasseur, Lucazeau & Bayer 1986; Nielsen 1986; Wang & Beck 1987; Beck & Shen 1989). In this paper, we use a boundary flux updating procedure which simplifies the computation.

Some preliminary results of the application of the generalized non-linear inverse method to the problems of coupled hydrological and thermal regimes are presented in a paper by Wang, Shen & Beck (1989), which will hereafter be referred to as Paper I. The method has two major steps—parameterization and parameter estimation. An outline of the finite element parameterization and a discussion of the Bayesian parameter estimation are made in Paper I. Synthetic examples show that with reasonably sufficient and well-distributed data, material properties and field variables can be resolved. Complementary to, and as a continuation of, that work, the present paper has a two-fold purpose: (1) to provide a more detailed mathematical development of the finite element discretization and the formulation of the gradient matrix required by the optimization procedures of the inverse method; (2) to complete the study of boundary flux updating, which may be considered as the third step of the method, and to illustrate, using numerical examples, its applications to the determination of the basal HFD, that is the conductive contribution to the heat flow, in hydrologically active regions.

Details of the parameter estimation method are given in Paper I, but a brief recapitulation is given in the next section; after this, the method of parameterization is developed in more detail. Then, we describe the procedures of updating boundary fluxes. Finally, a numerical example with simple geometry and variable data input is presented to illustrate the application of the boundary flux updating technique to the determination of basal HFD in hydrologically active areas.

A SOLUTION TO BAYESIAN NON-LINEAR INVERSE PROBLEMS

If a parameter vector $\mathbf{p}$ and a 'data' vector $\mathbf{f}$ are related by a deterministic theoretical relation in the form of a set of mildly non-linear vectorial functions $\mathbf{g}(\cdot)$, we write,

$$\mathbf{g}(\mathbf{p}) = \mathbf{f}. \tag{1}$$

If the *a priori* probability density function (PDF) of $\mathbf{p}$, $\mathcal{P}(\mathbf{p})$, with the covariance matrix C_{pp}, and the conditional PDF of $\mathbf{f}$ given $\mathbf{p}$, $\mathcal{P}(\mathbf{f} \mid \mathbf{p})$, with the covariance matrix C_{ff}, are both assumed to be jointly Gaussian, then, under favourable conditions, the following iteration scheme by Rodgers (1976) and Tarantola & Valette (1982) (called the RTV scheme in the rest of the text) converges to $\hat{\mathbf{p}}$, the most probable Bayesian estimate of $\mathbf{p}$,

$$\hat{\mathbf{p}}_{\mathbf{k}+1} = \mathbf{p}_0 + C_{pp} \cdot G_{\mathbf{k}}^t \cdot \mathbf{Y}_{\mathbf{k}} \tag{2a}$$

with

$$\mathbf{Y}_{\mathbf{k}} = R_{\mathbf{k}}^{-1} \cdot [\mathbf{f}_0 - \mathbf{g}(\hat{\mathbf{p}}_{\mathbf{k}}) + G_{\mathbf{k}} \cdot (\hat{\mathbf{p}}_{\mathbf{k}} - \mathbf{p}_0)] \tag{2b}$$

$$R_{\mathbf{k}} = C_{ff} + G_{\mathbf{k}} \cdot C_{pp} \cdot G_{\mathbf{k}}^t. \tag{2c}$$

The right superscript t denotes transpose operation; bold faced subscript $\mathbf{k}$ represents the iteration step numbers; $\hat{\mathbf{p}}_{\mathbf{k}}$ is the estimate of $\hat{\mathbf{p}}$ at the $\mathbf{k}$th iteration; $\mathbf{p}_0$ is the expectation of the *a priori* PDF of $\mathbf{p}$, $\mathbf{f}_0$ the known value (one realization) of $\mathbf{f}$, and G the gradient (Jacobian) matrix of the transformation (1), defined as

$$G_{\mathbf{k}} = (G_{lm})_{\mathbf{k}} = \left(\frac{\partial g_l}{\partial p_m}\right)\Bigg|_{\mathbf{p}=\hat{\mathbf{p}}_{\mathbf{k}}}. \tag{3}$$

For a large non-linear problem, the *a posteriori* covariance matrix $\hat{C}_{pp}$, of $\mathbf{p}$, would be extremely difficult to obtain; the usual approach is to linearize $\mathbf{g}(\mathbf{p})$ at $\hat{\mathbf{p}}$ and approximate $\hat{C}_{pp}$ with that of a linear case, given by the following equation (Schweppe 1973; Rodgers 1976; Tarantola & Valette 1982),

$$\hat{C}_{pp} = C_{pp} - C_{pp} \cdot G^t \cdot R^{-1} \cdot G \cdot C_{pp}. \tag{4}$$

The updated 'data' vector $\hat{\mathbf{f}}$ is given by

$$\hat{\mathbf{f}} = \mathbf{g}(\hat{\mathbf{p}}) \tag{5}$$

with the covariance matrix, also as a linear approximation,

$$\hat{C}_{ff} = G \cdot \hat{C}_{pp} \cdot G^t. \tag{6}$$

A discussion of the Bayesian non-linear inverse method was given in Paper I at length, so here we only briefly summarize a few important points.

(1) For a linear Bayesian inverse problem based on Gaussian distribution, a point estimate, such as the expectation, is adequate to represent the *a posteriori* PDF of the parameter vector; but for a non-linear problem, it may not be, because the *a posteriori* PDF may behave in a very complex manner (Box & Tiao 1973). Schweppe (1973) summarized four types of point estimates for non-linear Bayesian problems, each revealing a different aspect of the *a posteriori* PDF, namely, the most probable, the conditional mean, the median and the min–max estimates (for definitions, refer to Schweppe 1973, p. 329). The most probable estimate, used in this work, gives identical results to that of the maximum likelihood method (Menke 1984, p. 147) and is usually the easiest to compute.

(2) To use the *a posteriori* convariance matrix (4) to approximate that of a non-linear case implies the use of the most probable estimate to approximate the *a posteriori* expectation of the parameter vector in this work. This is justified only when the problem is mildly non-linear.

(3) Iteration scheme (2) can be derived by applying Newton's method for solving non-linear algebraic systems to the maximization of the *a posteriori* PDF of the parameter vector (Rodgers 1976; Wang & Beck 1987). As a Newton iteration scheme, it converges quadratically to a unique solution when the problem is mildly non-linear and the initial value is not too far away from the solution. Given the function form (1), the convergence behaviour of the iteration scheme is determined by the quality of the *a priori* information.

FINITE ELEMENT DISCRETIZATION

The physical laws governing the subsurface thermal and hydrological regimes and their interactions include Fourier's law of heat conduction, Darcy's law of macroscopic fluid flow in porous media, the law of energy conservation and the law of mass conservation, etc. At steady state, the mathematical expressions for these laws are the following set of coupled partial differential equations (e.g. Bear 1972),

$$\frac{\partial}{\partial x_i}\left(\lambda_{ij}\frac{\partial T}{\partial x_j}\right) - \rho c v_i \frac{\partial T}{\partial x_i} = 0 \tag{7}$$

$$\rho_0 g \frac{\partial}{\partial x_i}\left\{\frac{\kappa_{ij}}{\mu}\left(\frac{\partial h}{\partial x_j} + \rho_r \delta_{2j}\right)\right\} = 0, \tag{8}$$

where ρ_0 = the density of water at a reference temperature T_0, g = gravitational acceleration, T = temperature, h = reference hydraulic head defined as $(x_2 + P/\rho_0 g)$ where P is the fluid pressure, ρ_r = the relative water density, defined as

$$\rho_r = \frac{\rho - \rho_0}{\rho_0}, \tag{9}$$

ρ being the water density at temperature T, μ = dynamic viscosity of water, ρc = specific thermal capacity of water, taken as constant, δ_{ij} = Kronecker delta; the term in (8) containing δ_{2j} implies that the x_2 axis of our coordinate system is in the reverse direction of gravity, v_i = specific discharge or Darcian velocity of water, given by

$$v_i = -\frac{\kappa_{ij}}{\mu}\rho_0 g\left(\frac{\partial h}{\partial x_j} + \rho_r \delta_{2j}\right). \tag{10}$$

As a convention, a letter with subscript(s) $i, j, \ldots, n$ is used to denote the component of a vector or tensor unless otherwise specified, with subscripts i and j reserved for $\mathbb{R}^2$, i.e. $i, j = 1, 2$; for a vector, the same bold face letter but without a subscript is used to denote the matrix form of the vector. In the above equations and the rest of the text, repeated subscripts and superscripts $i, j, \ldots, n$ imply summation. For generality, the thermal conductivity λ and permeability κ are taken as tensors of the second rank in (7) and (8).

The reference hydraulic head h reduces to the usual hydraulic head as a water flow potential if the temperature dependence of ρ is assumed to be negligible. The assumption, though not made in this work so as to maintain generality, is reasonable for small Rayleigh number flow in porous media (Bejan 1984). However, the temperature dependence of μ must be taken into account for the temperature range of our problem, as pointed out in Paper I.

In this work, the temperature dependence of ρ and μ is given as a first-order approximation,

$$\rho = \rho_0 - \beta(T - T_0) \tag{11}$$

$$\mu^{-1} = \mu_0^{-1} + \eta(T - T_0), \tag{12}$$

where β and η are constants. A graphical comparison of the linear approximation and the actual $\rho - T$ and $\mu - T$ relation was given in Paper I. If better accuracy for ρ and μ, or a wide temperature range is required, it can be seen that multisection linear forms can replace (11) and (12). The numerical values of the parameter constants used in this work are listed in Table 1.

The inclusion of a source/sink term in equation (7), as done in Paper I, does not substantially complicate the problem, but does necessitate some special treatment in updating the boundary fluxes later in the inversion procedures. This term is not included here because (1) over the depth range (a few kilometres) considered in this work heat generation is usually insignificant, and (2) the symmetry of (7) and (8) will be maintained thus making the following derivation concise.

To use a discrete parameter estimation technique to estimate a spatially or temporally variable physical quantity, whether it is a field variable or a material property, a finite number of parameters that are sufficiently representative of the quantity must be found. This process, known as discretization or parameterization, is usually the first step of an inverse method. Since dimensionality is reduced from an infinite to a finite number, assumptions and approximations are usually necessarily invoked. The parameterization of a

Table 1. A list of parameter constants used in equations (7), (8), (11) and (12).

Constant	Value	Unit
T_0	30	°C
ρ_0	995.91	kg m^{-3}
β	0.53625	kg m^{-3} K^{-1}
μ_0^{-1}	1253.1	s m kg^{-1}
η	32.579	m s kg^{-1} K^{-1}
ρc	4.18×10^6	J m^{-3} K^{-1}
g	9.8	m s^{-2}

physical quantity can be performed in two different ways, probabilistic or deterministic.

From a probabilistic point of view, the material properties and/or field variables are regarded as realizations of random fields or spatial stochastic processes. With certain stationarity assumptions, these physical quantities are described by statistical moments. The concept of random field is much used in the study of groundwater hydrology (Hoeksema & Kitanidis 1985a; Dagan 1986); an example in terrestrial heat flow research can be found in Nielsen (1987). In the inverse formulation of Kitanidis & Vomvoris (1983) and Hoeksema & Kitanidis (1984, 1985b), the parameters to be estimated are the unknown coefficients in both the trend in the mean of the logarithmic hydraulic conductivity and the covariance function of its residual. The covariance matrix of the hydraulic head and log-conductivity values is formed through the use of a stochastic partial differential equation relating the two variables. An apparent advantage of the probabilistic approach is that a very small number of parameters are used while the arbitrary heterogeneity of the material property is still accounted for.

Any inverse solution by statistical parameter estimation is probabilistic, but many parameterization methods do not have to invoke the concept of random fields, and can be formally performed in a deterministic manner. With a deterministic approach, a physical quantity can be mapped on to a function space with a finite number of basis functions. The parameters to be estimated are usually the generalized coordinates of the bases. The simplest basis functions are step functions, and a generalized coordinate is the average value of the variable over the corresponding step length (or block, for more than one dimension) (Jackson 1979). In the usual finite element formulation in hydrological inverse methods (Cooley 1977; Neuman & Yokawitz 1979; Sun & Yeh 1985; Carrera & Neuman 1986; Woodbury & Smith 1988), material properties are parameterized using step functions, that is, each element or a group of elements is assigned the same material property value (zonation); the field variables, on the other hand, are parameterized using the polynomial basis functions, with the generalized coordinates being the nodal values of the variables (interpolation). In some cases, the material properties are chosen to be interpolated using basis functions and nodal values (Yeh & Yoon 1981). There are numerous other ways of deterministic parameterization; almost any numerical technique can be listed as an example.

Although conceptually very different, the two approaches are closely related in certain ways. If the generalized coordinates based on step-functions are viewed as random variables, they can be considered as approximations to a spatial stochastic process if the correlation between the steps are appropriately defined; the goodness of the approximation depends on the size of the steps (blocks). This fact permits the use of Monte Carlo methods in the analysis of spatial variability of the physical properties of subsurface porous media (Freeze 1975; Smith & Freeze 1979). Similarly, the discrete spectrum representations of a time or space series in the inverse methods of Gavalas, Shah & Seinfeld (1976) and of Wang & Beck (1987) can be regarded as either probabilistic or deterministic. In fact, any deterministic parameterization method can find a probabilistic interpretation. For example, one may regard zonation as probabilistic, saying that the material property is a stochastic process that has a perfect autocorrelation in each zone; one may also regard interpolation as probabilistic, maintaining that it is the first moment of the stochastic process that is interpolated. A comparison made by Kuiper (1986) shows that the deterministic approach based on finite elements, despite its simplicity, may perform as well as or better than the probabilistic approach based on statistical moments in 2-D inverse groundwater modelling problems.

In this work, we choose the deterministic approach and parameterize the problem with a 2-D isoparametric finite element model. With this model, the spatial domain of our problem is first divided into a number of quadrilateral elements, each having N_e (up to eight) nodes. Each element has a constant λ and κ value. The quadrilateral in the coordinate system $\mathbf{x}$ is mapped on to a square in the coordinate system $\mathbf{r}$, both in real space $\mathbb{R}^2$, by using a set of basis (or shape, interpolation) polynomial functions $\mathbf{H}(\mathbf{r})$,

$$x_i(\mathbf{r}) = H_k(\mathbf{r}) x_{ik}, \tag{13}$$

where subscript k stands for the global number of a node of the element, and the summation is over all the nodes the element has; x_{ik} denote the x_i coordinates of node k. The shape functions H_k for four-to-eight-node elements are given by Bathe & Wilson (1976). The values of field variables T and h at any point $\mathbf{r}$ in the element are interpolated by the same shape functions using the nodal values T_k and h_k,

$$T = H_k T_k \tag{14}$$

$$h = H_k h_k. \tag{15}$$

Transformation (13), i.e. $\mathbf{x} = \mathbf{x}(\mathbf{r})$ is 1–1 on $\mathbb{R}^2$, and hence there exists an inverse transformation $\mathbf{r} = \mathbf{r}(\mathbf{x})$, which means that (14) and (15) actually perform the interpolation in the $\mathbf{x}$ domain. For this reason, we are able to derive the finite element discretization to (7) and (8) in a common way without worrying about the isoparametric model, which is employed to (1) make the construction of a finite element mesh very flexible, (2) make the integrations required in the computation of conductivity and gradient matrices (see following text) very efficient, and (3) obtain a higher degree of interpolation of field variables than with the commonly used linear triangular model and hence better discretization accuracy can be achieved with fewer nodal points and elements.

Applying the Galerkin weighted residual method (e.g. Zienkiewicz 1972) to (7), we have, for element e,

$$\int_{\Omega^e} H_l \left(\frac{\partial}{\partial x_i} \lambda_{ij} \frac{\partial T}{\partial x_j} - \rho c v_i \frac{\partial T}{\partial x_i} \right) d\Omega = 0 \tag{16}$$

$l = 1, 2, \ldots, N_e$; where the integration is performed over the whole element domain Ω^e. Using Gauss' theorem, or integrating by parts, we obtain

$$\int_{\Omega^e} \left(\lambda_{ij} \frac{\partial H_l}{\partial x_i} \frac{\partial T}{\partial x_j} + H_l \rho c v_i \frac{\partial T}{\partial x_i} \right) d\Omega = \oint_{S^e} H_l \lambda_{ij} \frac{\partial T}{\partial x_i} n_j \, ds, \tag{17}$$

where s^e is the boundary path of the element, $\mathbf{n}$ is a unit vector normal to s^e pointing outwards from the element domain.

If we define heat flux going into the element as positive,

that going out as negative, the heat flux input at an elemental boundary point is then

$$q^h = -q_j^h n_j = \lambda_{ij} \frac{\partial T}{\partial x_i} n_j. \tag{18}$$

Substitution of (10), (14), (15) and (18) into (17) yields

$$\int_{\Omega^e} \left[\lambda_{ij} \frac{\partial H_l}{\partial x_i} \frac{\partial H_k}{\partial x_j} - \rho c \frac{\kappa_{ij}}{\mu} \rho_0 g \left(\frac{\partial H_m}{\partial x_j} h_m + \rho_r \delta_{2j} \right) H_l \frac{\partial H_k}{\partial x_i} \right] d\Omega \cdot T_k = \oint_{S^e} H_l q^h \, ds. \tag{19}$$

Similarly, applying the Galerkin weighted residual method to (8), we have, after some manipulation,

$$\left(\int_{\Omega^e} \frac{\kappa_{ij}}{\mu} \rho_0 g \frac{\partial H_l}{\partial x_i} \frac{\partial H_k}{\partial x_j} d\Omega \right) h_k - \left(\int_{\Omega^e} \delta_{2j} \frac{\kappa_{ij}}{\mu} g \beta \frac{\partial H_l}{\partial x_i} H_k \, d\Omega \right) T_k = \oint_{S^e} H_l q^w \, ds, \tag{20}$$

where q^w is the water flux input at the elemental boundary, again with the inward going flux defined as positive, i.e.

$$q^w = -q_j n_j = \frac{\kappa_{ij}}{\mu} \rho_0 g \left(\frac{\partial h}{\partial x_i} + \rho_r \delta_{2i} \right) n_j. \tag{21}$$

The second term on the left-hand side of (20) appears because ρ is a linear function of T as given by (11).

Defining a vector U in the (T, h) plane,

$$U = \begin{bmatrix} {}^1U \\ {}^2U \end{bmatrix} = \begin{bmatrix} T \\ h \end{bmatrix} \tag{22}$$

we can combine (19) and (20) into

$$K_{lk}^e U_k = f_l^e, \tag{23}$$

where $\mathbf{f}^e$ is the elemental equivalent nodal flow (ENF) vector, with

$${}^1f_1^e = \oint_{S^e} H_1 q^h \, ds \tag{24}$$

$${}^2f_l^e = \oint_{S^e} H_l q^w \, ds \tag{25}$$

and K^e is the elemental conductivity matrix, the (l, k)th entry being

$$K_{lk}^e = \begin{bmatrix} {}^{11}K_{lk}^e & {}^{12}K_{lk}^e \\ {}^{21}K_{lk}^e & {}^{22}K_{lk}^e \end{bmatrix} \tag{26}$$

with

$${}^{11}K_{lk}^e = \int_{\Omega^e} \left(\lambda_{ij} \frac{\partial H_l}{\partial x_i} \frac{\partial H_k}{\partial x_j} - \rho c v_i H_l \frac{\partial H_k}{\partial x_i} \right) d\Omega \tag{27}$$

$${}^{12}K_{lk}^e = 0 \tag{28}$$

$${}^{21}K_{lk}^e = -\int_{\Omega^e} \kappa_{ij} \mu^{-1} g \beta \delta_{2j} \frac{\partial H_l}{\partial x_i} H_k \, d\Omega \tag{29}$$

$${}^{22}K_{lk} = \rho_0 g \int_{\Omega^e} \kappa_{ij} \mu^{-1} \frac{\partial H_l}{\partial x_i} \frac{\partial H_k}{\partial x_j} d\Omega, \tag{30}$$

where v_i is defined by (10), and μ^{-1} by (12), with the T and h values interpolated using (14) and (15). The above derivation is similar to that of Huyakorn & Pinder (1983, p. 204).

The global system

$$K \cdot \mathbf{U} = \mathbf{f} \tag{31}$$

is the combination of the elemental system (23) over all elements, with

$$K = \sum_e K^e \tag{32}$$

$$\mathbf{f} = \sum_e \mathbf{f}^e. \tag{33}$$

The non-linear algebraic system (31) is the discretized form of the partial differential equations (7) and (8). At the current stage of the study, only isotropic media are considered. In a system identification problem, the elemental material properties λ and κ, or their logarithmic transform

$$\gamma = \ln \lambda \tag{34a}$$

$$\psi = \ln \kappa \tag{34b}$$

are usually grouped into fewer distinct values according to our knowledge of the subsurface geological structure and formations (zonation), and regarded as parameters, while $\mathbf{U}$ and $\mathbf{f}$ are considered as 'data'. As mentioned earlier, the objective of this work is to develop a generalized inverse method that can readily accommodate different types of data and *a priori* information. For this reason, we define a parameter vector $\mathbf{p}$ that includes not only all the discretized (after zonation) γ and ψ, as defined by (34), but also all the nodal values of T and h as its components; and $\mathbf{f}$, which contains the information on boundary fluxes (equations 24, 25), is taken as the 'data' vector. Therefore, (31) is directly written into a standard form to which the RTV scheme can be applied,

$$\mathbf{g}(\mathbf{p}) = \mathbf{f}, \tag{35}$$

where

$${}^i g_l(\mathbf{p}) = {}^{ij}K_{lk}{}^j U_k. \tag{36}$$

With the parameter vector defined as above, it can be seen that the field variables and material properties are treated mathematically equally as parameters. Therefore 'inverse' has a generalized meaning; the term is used here simply because the solution is obtained through statistical parameter estimation. The 'knowns' are those parameters with good *a priori* information, the 'unknowns' are those with poor *a priori* information. Forward and system identification solutions are the special cases of the general solutions. An added advantage of our choice of the parameter vector is that it makes the derivation of the gradient matrix matrix G rather simple (as can be seen in Appendix A). The principal disadvantage is that large computer memory is needed due to the large number of parameters.

Having defined the parameter vector $\mathbf{p}$ and the ENF vector $\mathbf{f}$, and obtained the vectorial functions $\mathbf{g}(\mathbf{p})$ and the gradient matrix G, we use the RTV scheme to seek the most probable Bayesian estimate of $\mathbf{p}$, with which $\mathbf{f}$ in turn can be updated. The parameter estimation procedure constrains the parameters by incorporating information in terms of their *a*

priori PDF. Aspects of the *a priori* and *a posteriori* PDFs are discussed in Paper I.

UPDATING BOUNDARY FLUXES

General remarks

The method developed in the previous sections is a generalized inverse approach. Given good information on the material properties and boundary conditions, forward calculation is performed to provide knowledge of the field variables, even though the method is called inverse. If there are data on the field variables and boundary conditions, the method can be used for system identification and to estimate the material properties. When the rock permeability or hydraulic conductivity is the major concern, thermal data can be used to provide further constraints on the hydraulic parameters, as already demonstrated by Woodbury & Smith (1988).

A major objective of the technique described in this paper is to find the background conductive HFD from deeper parts of the Earth's crust, from which the thermal structure of the lithosphere can be inferred. There are a number of sources of perturbation to the 'conductive' regime, e.g. surface topography, surface temperature variations, subsurface structure, groundwater flow, etc. In this section, a procedure is developed for updating boundary fluxes and is demonstrated by application to the determination of basal HFD in hydrologically active regions. Although only the hydrologic perturbations to the thermal regime are considered in this work, the method can be readily adapted to the downward continuation of heat flow data or, more simply, to correcting heat flow data for topography and structure.

Corresponding to the Dirichlet and Neumann boundary conditions in a forward solution to equations (7) and (8), the boundary condition in our inverse method can be constructed in terms of either boundary variable values or boundary fluxes. In some cases, boundary fluxes are difficult to specify and of little interest to us; for example, it is more convenient to use the water table rather than the discharge rate as a ground surface boundary condition for hydraulic head. Such Dirichlet conditions can be easily applied and updated. Here we consider the Neumann-type boundary conditions. At some boundaries, flux distribution can be reasonably well specified through actual field measurements; for example, the HFD pattern at the ground surface can be found from field measurements of temperature gradient and thermal conductivity. At some other boundaries, the flux distribution is to be determined by the inversion, for example, the basal HFD. In both cases, the boundary condition can be constructed in terms of boundary fluxes. If well known *a priori,* they will constrain the inversion; if poorly known *a priori,* they are to be resolved by the inversion. The latter situation is the major concern of this section.

Boundary flux updating procedure

The ENF vector $\mathbf{f}$ is formed through the integration of boundary fluxes, as given in equations (24) and (25), that is

$$f_i^e = \int_{S^e} H_i(s) \cdot q \, ds. \tag{37}$$

For conciseness, we neglect the left superscript of f, i.e. 1 and 2, and the right superscript of q, i.e. h (heat) and w (water). Therefore, the following derivation is applicable to the boundary fluxes of both heat and water. The continuous input boundary fluxes are sampled and given at the boundary nodes as distinct values q_k, but in (37), q is a continuous function of $\mathbf{x}$, or $\mathbf{r}$. To perform the integration (37), we interpolate the fluxes at any elemental boundary point $\mathbf{x}$ using q_k and the interpolation functions H_k

$$q = H_k q_k. \tag{38}$$

At one side of a quadrilateral isoparametric element used in this work there are not more than three relevant interpolation functions associated with the existing nodes. Substituting (38) into the integrand of (37) gives

$$f_i^e = \int_{S^e} H_i H_k q_k \, ds = \left(\int_{S^e} H_i H_k \, ds \right) \cdot q_k \tag{39}$$

or in matrix form

$$\mathbf{f}^e = V^e \cdot \mathbf{q}, \tag{40}$$

where the symmetric matrix

$$V^e = \int_{S^e} \mathbf{H} \cdot \mathbf{H}^t \, ds \tag{41}$$

is called the elemental boundary flow transformation matrix. It is not difficult to see that the global V matrix is the summation of the elemental V^e-matrices.

Therefore, the boundary nodal flux vector $\mathbf{q}$ is linearly transformed into the global ENF vector $\mathbf{f}$, i.e.

$$\mathbf{f} = V \cdot \mathbf{q}. \tag{43}$$

If $\mathbf{q}$ is Gaussian, $\mathbf{f}$ is also Gaussian, and the covariance matrix of $\mathcal{P}(\mathbf{f} \mid \mathbf{p})$ is readily obtained

$$C_{ff} = V \cdot C_{qq} \cdot V, \tag{44}$$

where C_{qq} is the covariance matrix of $\mathbf{q}$. The diagonal entries of C_{qq}, the variances, represent the uncertainties in the boundary fluxes; the off-diagonal entries, the covariances, define the spatial correlations between different components of $\mathbf{q}$.

If the covariances in C_{qq} are used to define the degree of smoothness of the flux distribution at a boundary, an extensively used exponential correlation function

$$\sigma_{lk}^2 = \sigma^2 \exp\left(-\frac{1}{2} \frac{S_{lk}^2}{L^2} \right) \tag{45}$$

can be used; here σ_{lk}^2 is the covariance between the two components of $\mathbf{q}$, q_l and q_k, separated by a distance S_{lk}, σ^2 the uniform variance of the components of $\mathbf{q}$ at this boundary, and L the correlation length. It is the correlation length that determines the degree of smoothness of the flux distribution at this boundary.

The updated ENF vector $\hat{\mathbf{f}}$ is given by equation (5). From (43), a linear inversion of the components of the updated $\mathbf{f}$ will give the updated boundary flux vector $\hat{\mathbf{q}}$. $\mathbf{f}$ and $\mathbf{q}$ are of the global dimension, i.e. twice the total number of nodal points. Some discussion is required to clarify the existence of V^{-1}. Because nodal points that are not on the global boundary, the inner nodal points, do not participate in

forming the global V matrix, most of the rows and columns of V consist only of zeros; this would make the V matrix singular, but it is not the only form of the V matrix. Consider an inner nodal point l at which

$$f_l = q_l \equiv 0. \tag{46}$$

If an arbitrary non-zero number is placed at the corresponding diagonal entry of the V matrix, so that $V_{ll} \neq 0$, equation (46) is still satisfied. Therefore, we can always ensure that V is non-singular by letting all the diagonal entries corresponding to inner points be non-zero. In real computation, this problem is easily avoided by neglecting the inner nodal points thus reducing the dimension of V, $\mathbf{f}$ and $\mathbf{q}$. Since V^{-1} exists, the updated boundary flux vector $\hat{\mathbf{q}}$ is obtained as

$$\hat{\mathbf{q}} = V^{-1} \cdot \hat{\mathbf{f}}. \tag{47}$$

From (47), the covariance matrix of $\hat{\mathbf{q}}$, $\hat{C}_{qq}$, is

$$\hat{C}_{qq} = V^{-1} \cdot \hat{C}_{ff} \cdot V^{-1} \tag{48}$$

so that, according to (6),

$$\hat{C}_{qq} = V^{-1} \cdot G \cdot \hat{C}_{pp} \cdot G^t \cdot V^{-1}. \tag{49}$$

$\hat{C}_{qq}$ can be put into another form which is similar to that of $\hat{C}_{pp}$ as given by equation (4) (see Appendix B),

$$\hat{C}_{qq} = C_{qq} - C_{qq} \cdot V \cdot R^{-1} \cdot V \cdot C_{qq}. \tag{50}$$

This makes the computation of $\hat{C}_{qq}$ very efficient, because we can choose to compute only those entries of $\hat{C}_{qq}$ that are related to the boundary fluxes that interest us, such as the basal HFD, and also avoid the time consuming computation of $\hat{C}_{pp}$ and $\hat{C}_{ff}$.

The updated boundary flux $\mathbf{q}$ at any boundary point of an element is interpolated with the updated nodal values of boundary flux of the element using (38), i.e. in matrix form,

$$\hat{q} = \mathbf{H}^t \cdot \hat{\mathbf{q}}. \tag{51}$$

The variance of $\hat{q}$ is then

$$\hat{\sigma}_q^2 = \mathbf{H}^t \cdot \hat{C}_{qq} \cdot \mathbf{H}. \tag{52}$$

A NUMERICAL EXAMPLE OF BASAL HFD DETERMINATION

In this section, the boundary flux updating technique is applied to the determination of basal HFD in hydrologically active areas. Because it is necessary to know how close the inverse results are to a perfectly known situation, we choose to test against an idealized synthetic model rather than use a field example. With a synthetic model, it is also easy to understand the behaviour of the solution by isolating different factors that affect the results, and to find the limitations of the method by using input datasets with different noise levels. Once a satisfactory technique for solving the problem has been identified, it can be applied to real problems.

The idealized model used here is based on a small trough-type sedimentary basin. Fig. 1a shows the cross-section of the model to which our 2-D inverse method is applied. There are only three sedimentary formations, each having a distinct thermal conductivity and permeability

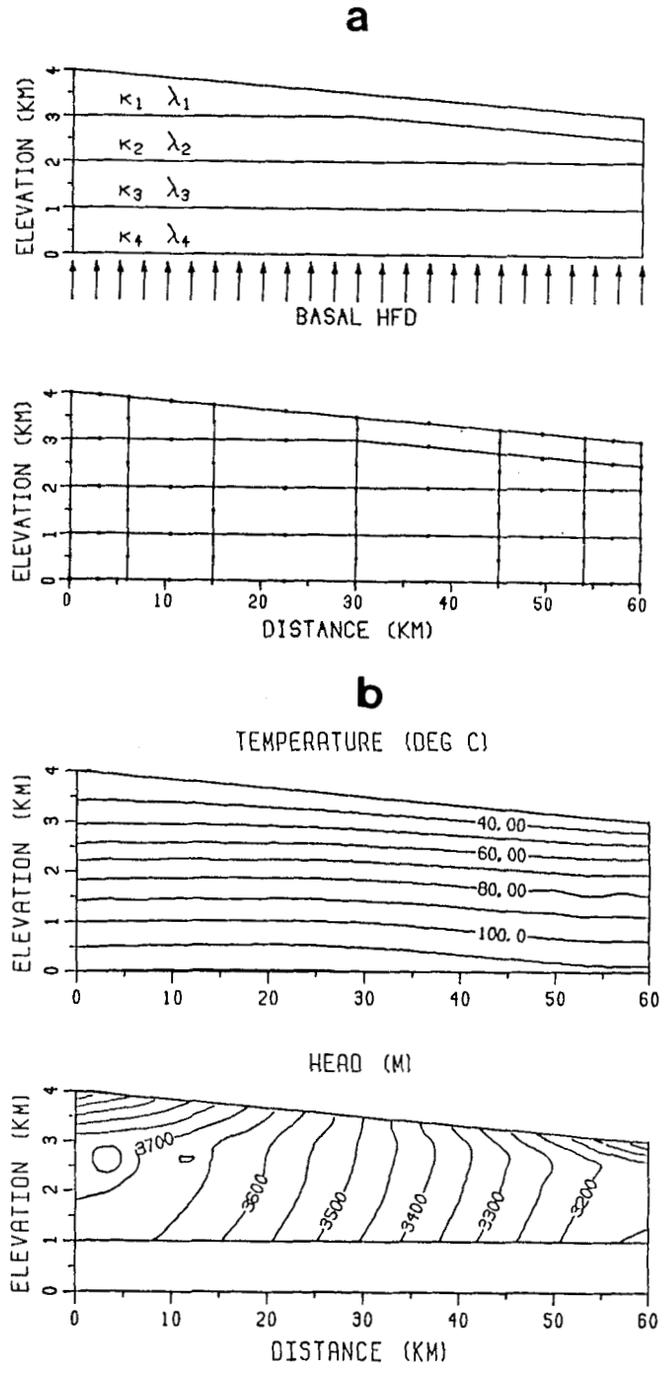

Figure 1. (a) A simple synthetic geological model and the finite element mesh used for the inverse solutions. The medium consists of four layered geological units, each of which has a distinct thermal conductivity and permeability value, as listed in Table 2. The finite element discretization in the vertical direction coincides with the geological units. (b) True model, for subsequent inversion, obtained in a forward solution of the simple geological model illustrated in (a); note that the reference hydraulic head as defined in the text is not a potential, and is therefore difficult to interpret visually.

value (Table 2), overlying an impermeable crystalline basement. The first (top) geological unit is an aquitard, the second unit is the major aquifer in the system, and the third unit is a less permeable aquifer. Part of the basement is included in the model as the fourth layer to minimize the

Table 2. Material property values of the synthetic geological model (refer to Fig. 1(a) for the zone numbers).

Zone number	λ value ($W m^{-1} K^{-1}$)	κ value ($10^{-16} m^2$)
1	2.0	0.5
2	2.0	100.0
3	2.5	10.0
4	3.0	0.0

influence of the thermal disturbance by water flow in the overlying permeable rock units on the lowermost boundary of the model, where the conductive HFD from below is assumed to be unperturbed. The geometrical and structural simplicity of the geological model removes the need to take into account perturbing factors such as the effects of topographic relief and 3-D structure and makes it relatively easy to demonstrate the general features of the inverse solutions to our specific problem. Naturally, for a more complex model, more material property zones and a finer finite element mesh should be employed and, ultimately, a 3-D model will be needed; with the isoparametric finite element model, these extensions are not difficult in principle but are computationally more expensive.

Synthetic data of field variables T and h, are generated with given material property values (Table 2) and appropriate boundary conditions by using a forward finite element calculation, a procedure similar to that of Smith & Chapman (1983). The nodal values of the temperature and head fields obtained by the forward calculation are shown in Fig. 1b. These values, together with the logarithmic transform of λ and κ values, are taken as the true values of the components of the parameter vector **p**. The true basal HFD from the bottom of the cross-section is taken to be a constant at a typical value of $60 mW m^{-2}$. The 'measured' ground surface HFD, as well as its noise level, is a function of position (Fig. 2), and the water table is assumed to coincide with the ground surface; these surface boundary conditions are used in all the numerical experiments. The nodal values of these functions and of the guessed basal HFD consist of the non-zero components of the nodal

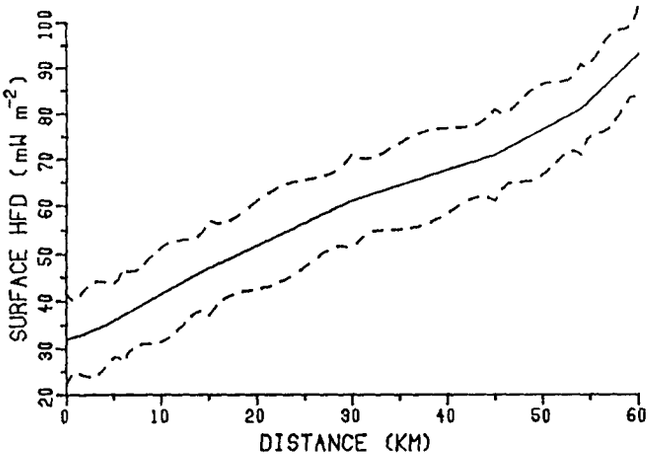

Figure 2. The near-surface HFD distribution used as the upper thermal boundary condition for all the inverse solutions. The dashed lines represent 1 s.d. error range.

boundary flux vector **q**. The two vertical boundaries are assumed to be impermeable perfect insulators. Our 'field data' are the values of the parameter vector **p** and the boundary flux vector **q** together with their standard deviations.

With reasonably well-known boundary heat fluxes, the inverse method can resolve the field variables and material properties using noisy data. For example, consider a situation where the basal HFD is correctly known to be $60 mW m^{-2}$ with a standard deviation (s.d., but STD on the figures) of only $1 mW m^{-2}$, but the values of material properties are unknown. To indicate our lack of knowledge of the material properties, we assign *a priori* lognormal PDFs with erroneous *a priori* expectations and large s.d., that is, the values are very loosely constrained. The nodal values of T and h obtained from the forward solution are perturbed by Gaussian random noise (Fig. 3a and b), and then regarded as the field data. The availability of accurate measurements and the certainty in the data usually decreases with increasing depth; to account for this, the noise added to the nodal values of T and h are given as increasing with depth, as shown by the contour maps of the s.d. of T and h (Fig. 3a and b). The solution shows that the estimates of most of the parameters are close to their true values, the reliability decreasing with depth, as illustrated in Fig. 3. There is not much information gain on the permeability of the third layer where the head data are very noisy. Being non-linear, the power of this inverse method is limited by the noise level in the input data. In the current system identification problem, for example, if the noise in the *a priori* nodal values of T and h is increased by 25 per cent, an almost identical solution can be obtained; but if the noise is increased by 50 per cent, the iteration will not converge, unless better information on the material properties or on the boundary conditions are given. Because this is not one of the examples of applying the boundary flux updating technique to the background HFD problem, it is referred to as case 0.

In each of the following cases, the basal HFD is assumed to be very poorly known *a priori*, and a constant value of $70 mW m^{-2}$ is guessed at every lower boundary nodal point; a large s.d. of $40 mW m^{-2}$ is assigned to show our ignorance of the HFD value. The correlation length L of the basal HFD will be specified for individual examples. Numerical experiments show that with the basal HFD so loosely constrained, it does not matter whether a value of 70 or $80 mW m^{-2}$, a constant or a reasonable set of different values is used as the guess. By varying the noise level of other parts of the synthetic dataset, we are able to examine the information requirement and the limitations of the boundary flux updating technique when applied to the problem of HFD determination.

Case 1. Accurate field variable data

In this case, T and h data contain Gaussian random noise with very small s.d. of 0.001 K and 0.1 m, respectively, but the material property values of all geological units are assumed to be unknown. Our objective is to estimate the thermal conductivities and permeabilities of all the geological units and the basal HFD. This is a system identification problem with one very uncertain boundary

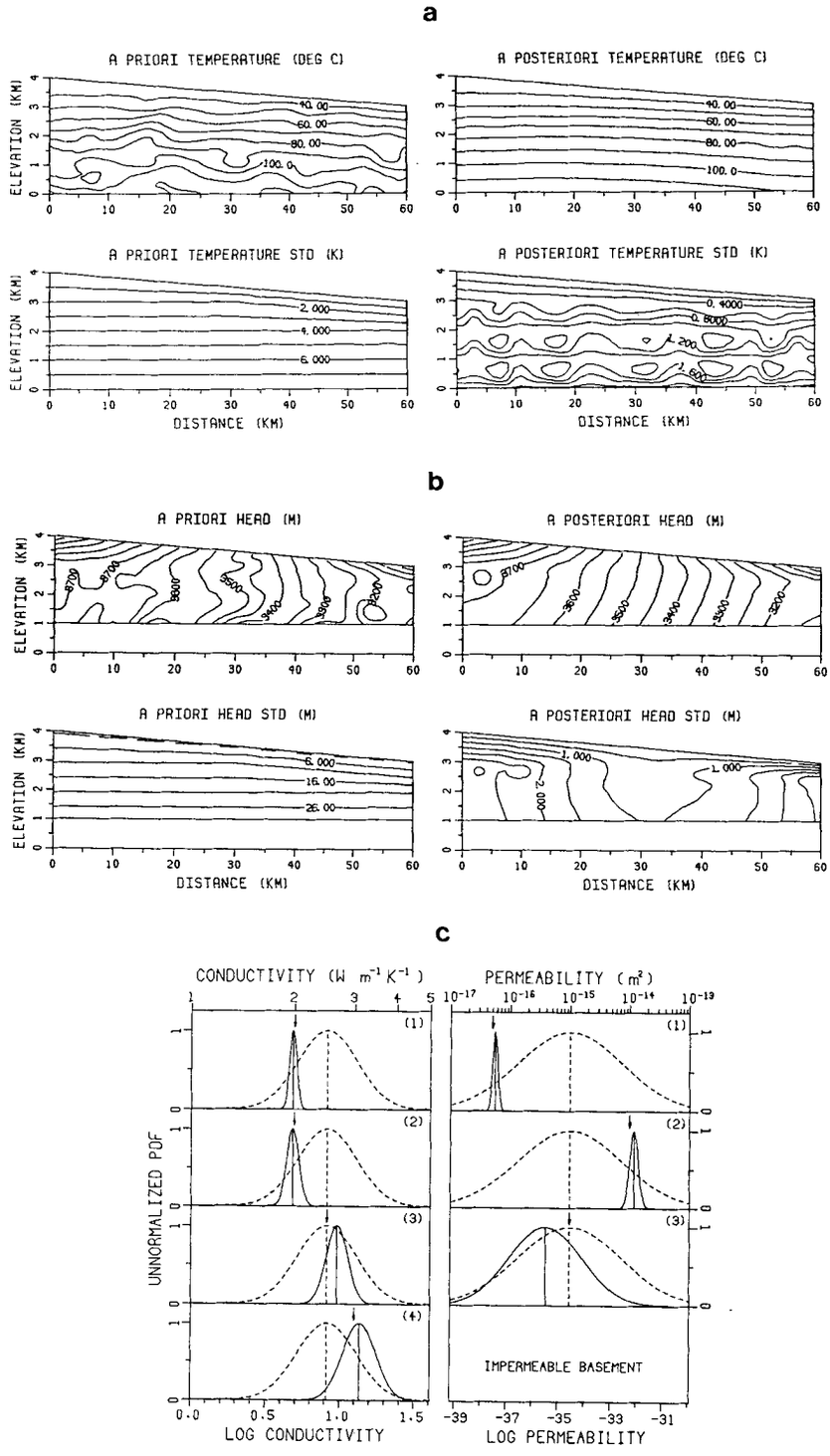

Figure 3. The inverse solution of case 0, in which the material property values are unknown and the s.d. of noise in temperature and head data increase with depth. (a) Contour maps of nodal values and s.d. for temperature. (b) Contour maps of nodal values and s.d.'s for head. (c) *A priori* (dashed lines) and *a posteriori* (solid lines) thermal conductivity and permeability PDFs showing that the material properties are resolved. The numbers in brackets are the zone numbers. The true property value, which a perfect inversion will return, of each zone is indicated by an arrow.

condition. Since it is assumed that nothing is known about the material property values, erroneous and loosely constrained homogeneous *a priori* values of λ and of κ for the whole medium are used (Fig. 4a); the correlation length of the basal HFD is taken to be zero. Here both the boundary heat flux and the thermal conductivities of the medium are poorly constrained, while the geothermal gradient is tightly constrained because the temperature field is almost noise free. For a pure heat conduction problem, it is easy to see from Fourier's law that if the temperature

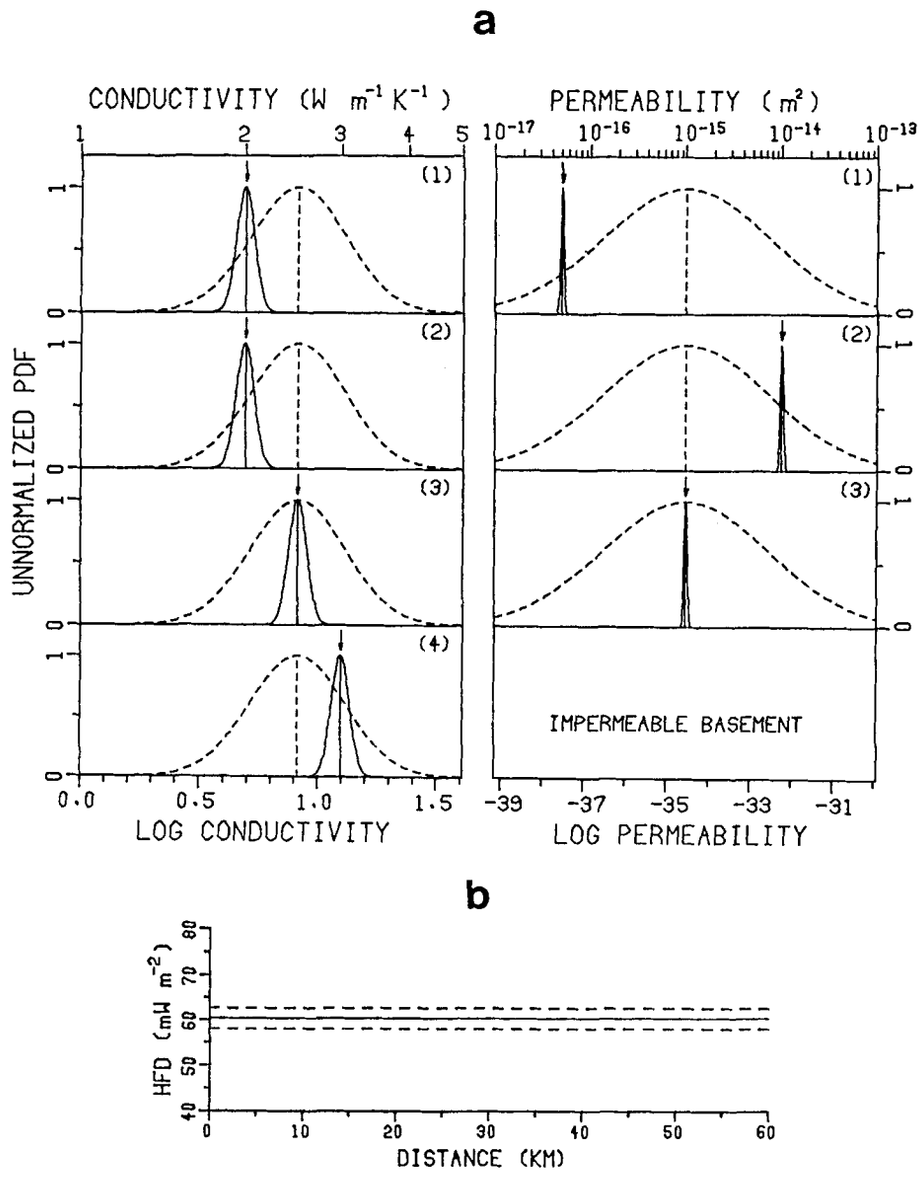

Figure 4. Inverse solution of case 1, in which the T (s.d. = 0.001 K) and h (s.d. = 0.1 m) data are nearly noise-free; λ and κ are unknown. (*A priori* (dashed lines) and *a posteriori* (solid lines) material property PDFs. (b) The updated basal HFD distribution.

gradient is the only physical quantity that is well constrained, an inverse method will tend to find a proper ratio of HFD and λ, as noted by Wang & Beck (1987) and Shen & Beck (1988). The current case involves convective heat transfer, and the head field and its boundary conditions, that is, the water table and the other three impermeable boundaries, are either well constrained or pefectly known. The good hydrological data provided independent information on the HFD and λ, and thus helped to resolve the basal HFD as well as the material properties (Figure 4a and b).

We briefly examine the response of the solution to the assigned *a priori* values of the material properties in this simple case. Although there could be an infinite number of combinations of different *a priori* λ and κ values, the general behaviour can be demonstrated, in Table 3, by varying κ only. Convergence is defined as the L_∞ norm of the difference parameter vector at iteration step l $\mathbf{p}_k - \mathbf{p}_{k-1}$, is less than 0.01 (SI units). As long as th

Table 3. Convergence behaviour of the solution for case 1, responding to different *a priori* permeability κ values (*a priori* thermal conductivity $\lambda = 2.5$ W m^{-1} K^{-1} in all cases).

κ value (m^2)	Log s.d. (m^2)	Convergence behaviour
10^{-9}	4.0	Non-convergent
10^{-10}	3.5	18 iterations
10^{-11}	3.5	16 iterations
10^{-12}	3.0	14 iterations
10^{-13}	2.5	11 iterations
10^{-14}	2.5	9 iterations
10^{-15}	2.0	7 iterations
10^{-16}	2.0	Non-convergent

iteration converged, it was found (results not shown) that all solutions were very similar to those shown in Fig. 4. It is interesting to see that a smaller *a priori* κ may easily render the solution unstable, but a larger value (up to 10^{-10}) only tends to cost more iteration steps.

Case 2. Accurate material property data

In this case, the λ and κ values are all accurately known, with lognormal s.d. of 0.001. The noise level of the T and h data is the same as in case 0 (Fig. 3a and b). The objective is to estimate the temperature and head field and the basal HFD. Because the material property values are accurately known and therefore well constrained, this case is similar to a forward solution of the problem except that one boundary condition, the basal HFD, is very uncertain. With this dataset and a zero correlation length of the basal HFD, the RTV iteration scheme converges to T and h values that are far from the true values in certain regions of the cross-section, as can be seen in the contour maps of the *a posteriori* nodal values of the temperature field (Fig. 5a); consistent with the incorrect temperature field, an incorrect basal HFD distribution has been estimated (Fig. 5b). The situation tends to be worse in the discharge and recharge regions where the vertical component of water movement is prominent and therefore, because the flow of heat in this model is mainly vertical, the thermal and hydrological regimes are strongly coupled. It can be observed in equations (7) and (8) that with given material property values, the more strongly coupled the two regimes are, the more non-linear the problem becomes, and hence the more difficult it is for an iteration scheme to converge to a correct solution (see earlier discussion on the RTV scheme). We refer to these regions as the 'sensitive' regions, since the solution there is more vulnerable to noise in the data. There are three ways to improve the results:

(1) In this synthetic case, spatially uncorrelated noise was added to the true nodal values of T and h to form a noisy

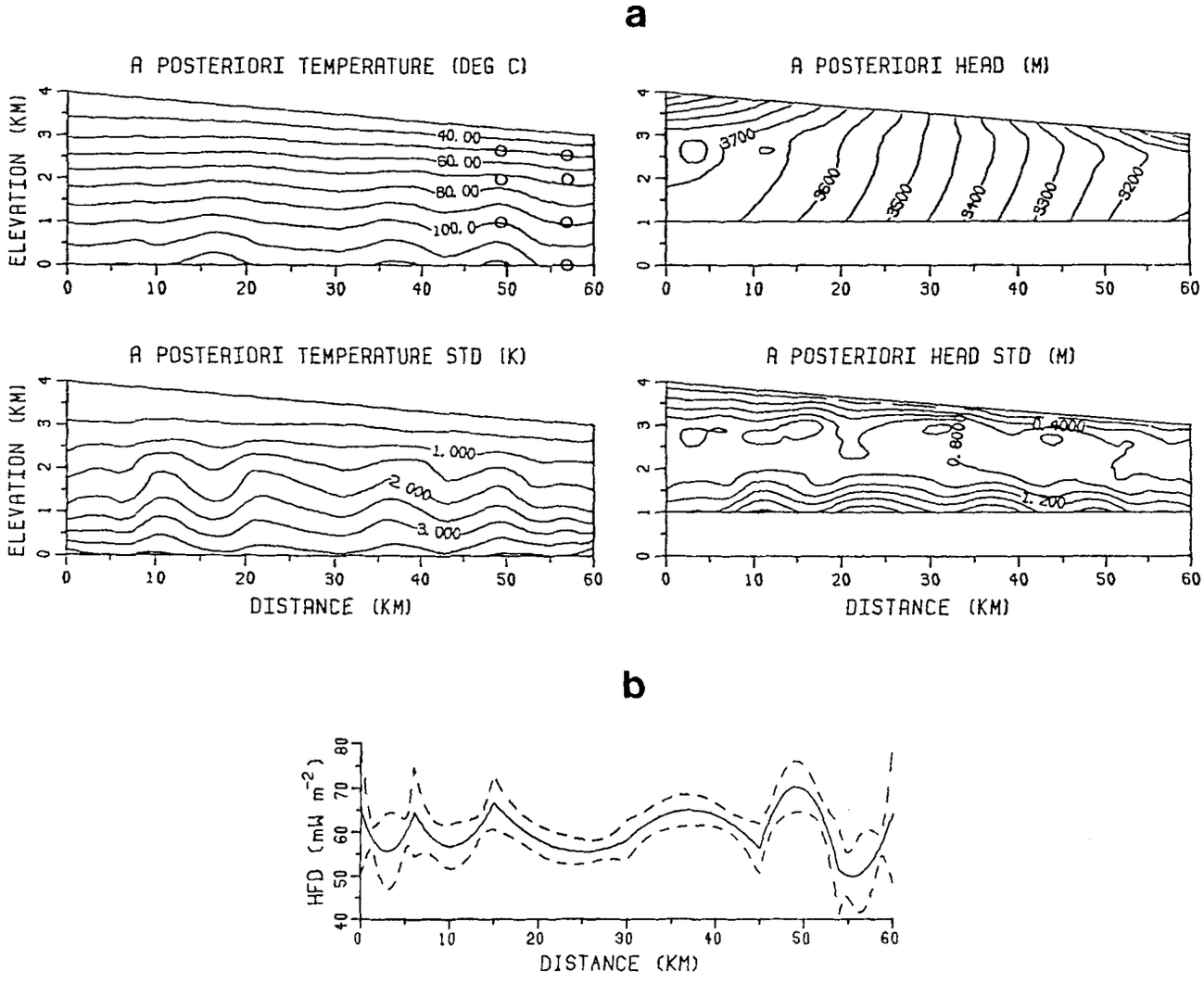

Figure 5. First inverse solution of case 2, in which the λ and κ values are all accurately known (log s.d. = 0.001), and the *a priori* T and h are the same as in case 0 (Fig. 3); correlation length $L = 0$. (a) Contour maps of the *a posteriori* T and h and the s.d.; the temperature contour map shows that the iteration has converged to some wrong values. (b) The updated basal HFD distribution; the unrealistic oscillations are due to the wrongly resolved temperature field. See Fig. 6(c) for explanation of circled points.

dataset, so that there are some drastic, and possibly unrealistic, variations in the *a priori* T and h patterns as can be seen in Fig. 3a and b. Since these T and h values are used as initial values for the iteration, the large magnitude errors in them will have an undue influence on the convergence if the problem is sufficiently non-linear. If the noise in the *a priori* nodal values of T and h is reduced by 50 per cent but the same variances are used, that is, the initial values are closer to the true solution although the uncertainties in these values are the same, the results will be improved (Fig. 6a). In a real case, data would likely be processed, e.g. filtered, before being used and hence be smoother than in this synthetic case. Spatial correlations of the input nodal values, which are sometimes obtained by the data-processing procedures, may also help to constrain the solution.

(2) The assumption of zero correlation length allows the basal HFD to have variations of short wavelengths. A correlation length $L > 0$ may smooth the results. The same case as shown in Fig. 5 was recomputed with $L = 10$ km, and the results were obviously improved (Fig. 6b). However, we have to be careful in specifying the value of L. Unless other information is available, either from theoretical or experimental studies, all we know about the spatial correlation of the HFD is that L is unlikely to be zero; if a large L is chosen, we must ensure that we do not inadvertently create and use extra information.

(3) Even without smoothing the data and without choosing $L > 0$, the solution can be greatly improved by tightly constraining a few temperature points in the sensitive regions; in a real case this would mean that we have to obtain a few accurate borehole temperatures there. For example, if the noise s.d. of nodal temperatures at the seven circled points illustrated in Fig. 5a are reduced to 0.005 K, while those of other nodal temperatures and the head values remain the same as before, the basal HFD is much better resolved in the discharge region (Fig. 6c); although similar comments apply to the recharge region, fewer accurate temperature points would be needed there because the thermal disturbance is less focused there.

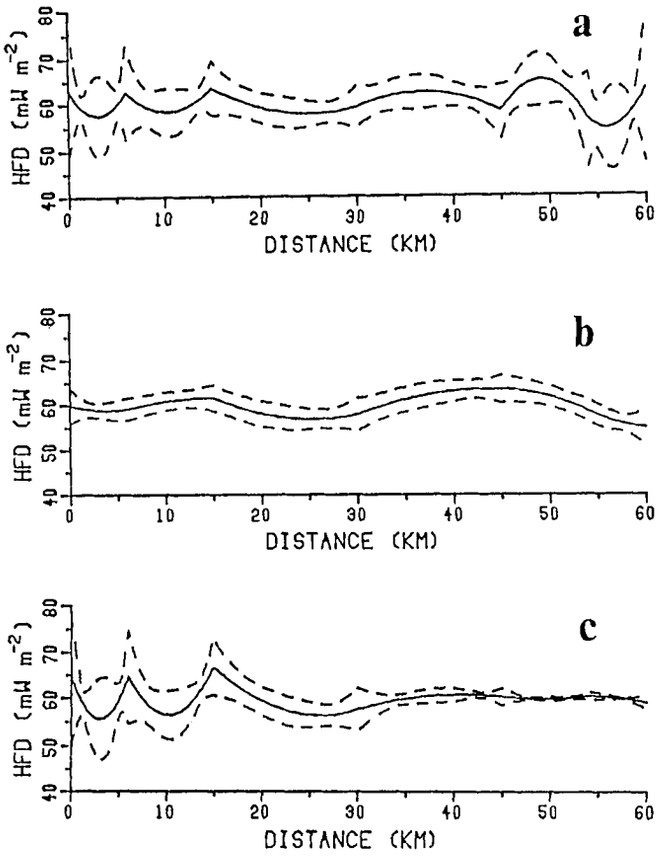

Figure 6. The updated basal HFD distribution of other solutions of case 2. (a) The noise in the *a priori* values of T and h is reduced by 50 per cent, although the same variances as before are used. (b) The correlation length of the basal HFD $L = 10$ km. (c) The seven-nodal temperature values indicated by circles in the discharge region in Fig. 5 are tightly constrained with s.d. = 0.005 K.

Case 3. Field variable and material property data with varying quality

In a realistic situation, some information is often available for all the physical quantities involved, but neither field variables nor material properties will be perfectly known, and the data quality varies from place to place in a study area. To test the inverse method for such a situation, the following case is considered.

Except for the temperatures at the 12 nodal points located in sensitive regions as illustrated by circles in the contour map of the *a posteriori* nodal temperatures in Fig. 7(a) which are tightly constrained with an s.d. of 0.005 K, the noise in the T and h data is the same as in case 0. Some of the material properties are better known while some are more poorly known *a priori* (Fig. 7b). It can be seen that the basal HFD (Fig. 7c), the field variables (Fig. 7a) and the material properties (Fig. 7b) are all well resolved.

Case 4. Accurate material property and head data, unknown temperature

This rather unrealistic but very interesting case is used to illustrate further the important feature of the inverse method, information compensation between different physical quantities.

The *a priori* information on the material properties is the same as in case 2, and the head data are the same as in case 1, but the temperature is assumed to be unknown. Ignorance of the temperature field is depicted by large noise in all the nodal temperatures with an identical s.d. as large as 50 K (Fig. 8a), which makes this field variable effectively unconstrained. Although the temperature data do not contribute to the inversion in a positive way, the basal HFD is still well resolved (Fig. 8b), because the lack of information on temperature is compensated by good knowledge of, and therefore well-constrained values of, head and material properties. A real situation is unlikely to be as extreme as in this case, but the principles of information compensation still prevail. However, information compensation is limited by the physical laws involved. Obviously, if the interaction between two physical quantities is weak, the information compensation link is also weak, as observed by Woodbury & Smith (1988). For example, if the order of magnitude of the second term in equation (7) is not comparable to that of the first term, due either to a low

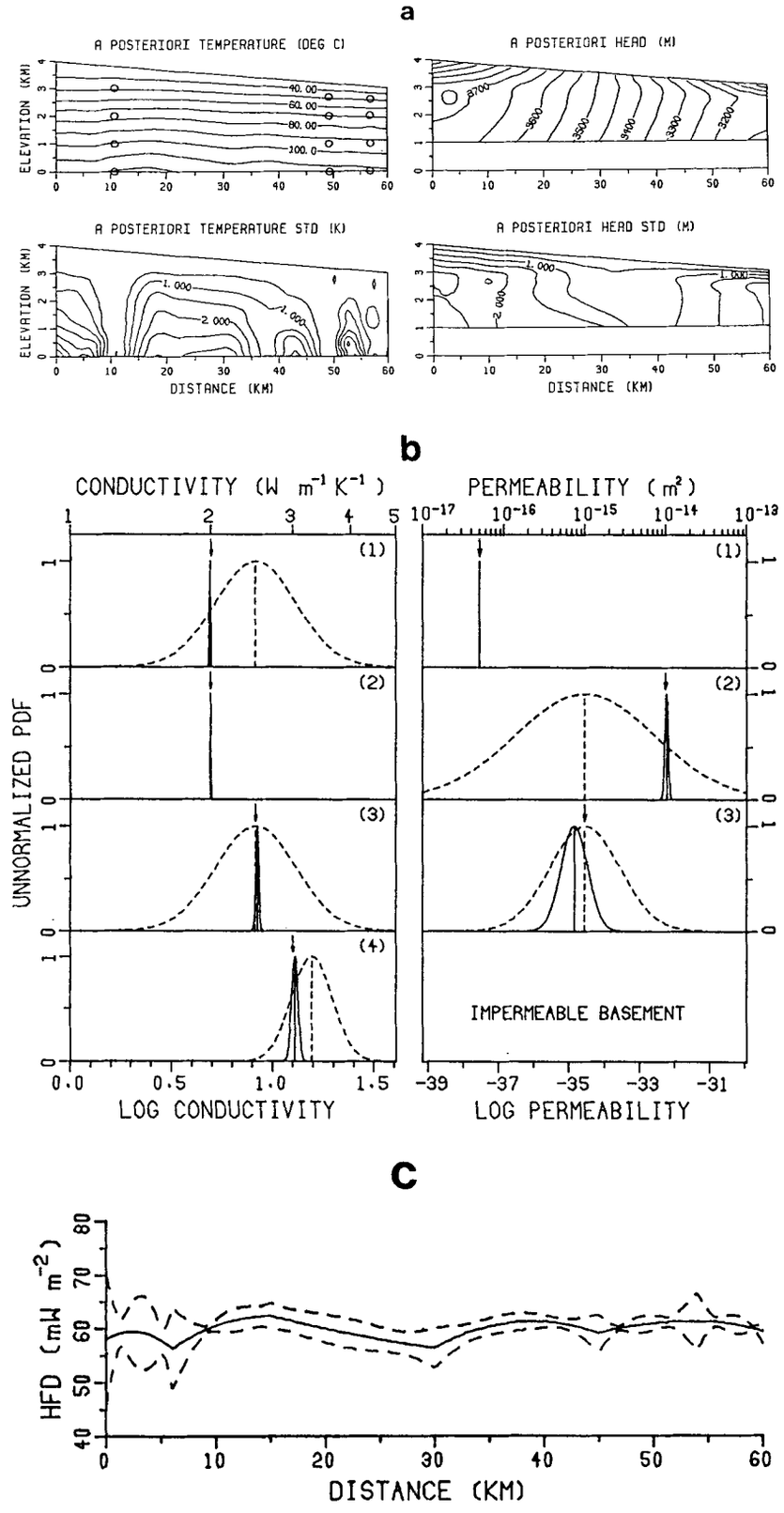

Figure 7. Inverse solution of case 3, in which the field variable data are the same as in case 0, except that the 12 nodal temperature points indicated by circles in the sensitive regions are tightly constrained with s.d. = 0.005 K. (a) Contour maps of the *a posteriori T* and *h* and the s.d.'s. (b) *A priori* (dashed lines) and *a posteriori* (solid lines) material property PDFs. (c) The updated basal HFD distribution.

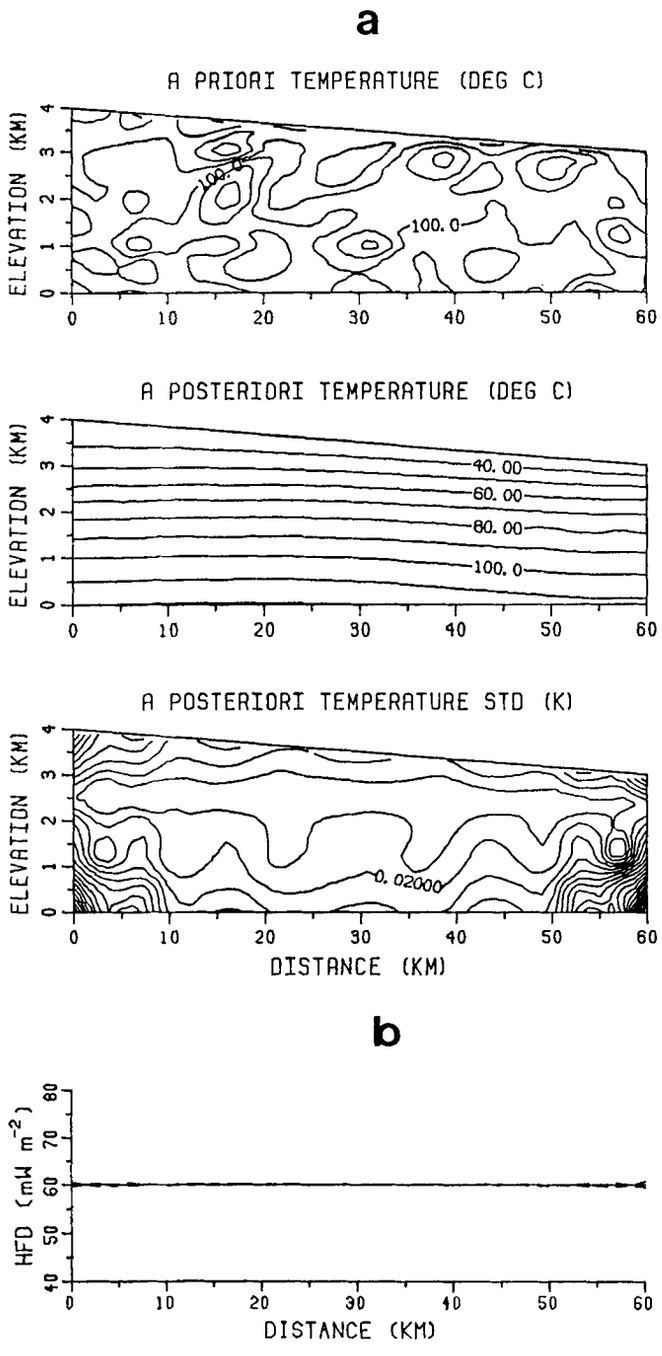

Figure 8. The inverse solution of case 4, with nearly noise-free head and material property data but very uncertain temperature data. The *a priori* s.d. for nodal temperatures is a uniform 50 K. (a) Contour maps of the *a priori* T and the *a posteriori* T and s.d.'s. The contour interval for the *a priori* temperature is 50 K. (b) The updated basal HFD distribution.

Darcian velocity or to the orthogonality of the Darcian velocity and the thermal gradient, little information on the temperature field would be extracted from the head values, even if they are perfectly known.

CONCLUSION AND DISCUSSION

A Bayesian type generalized non-linear inverse method is applied to the problem of coupled thermal and hydrological regimes, with the heat transfer equation and the fluid flow equation discretized by a 2-D isoparametric finite element model. All the finite element nodal values of temperature and head, and the logarithmic transform of the discretized thermal conductivity and permeability values are regarded as the components of a parameter vector. The 'data' vector of the usual Bayesian inference method is replaced with an equivalent nodal flow vector which is linearly transformed from boundary fluxes. The choice of the parameter vector, combined with a boundary flux updating technique, has two advantages:

(1) It makes the inverse method flexible in dealing with different types of problem and data quality. All three types of physical quantity involved (field variables, material properties, boundary fluxes) can be resolved by this method as long as there is a reasonable total amount of *a priori* information.

(2) It makes possible, and efficient, the application of a gradient method, such as the RTV scheme, to the maximization of the *a posteriori* joint PDF of the parameter vector.

A simple synthetic model is used to illustrate the application of the boundary flux updating technique to the determination of basal HFD in hydrologically active areas. Four cases with the same water-table configuration and uncertain ground surface HFD are investigated to see whether, and under what conditions, the very uncertain basal HFD can be resolved. In the first case, the field variable data are nearly noise-free, and it is possible to resolve the HFD when the material properties are unknown; in the second case, the material properties are accurately known while the random noise in the data of field variables increases with depth; in the third case, both field variable and material property data are moderately noisy; in the fourth case, an extreme situation is used to illustrate how the lack of information on one physical quantity can be compensated by good knowledge of other quantities. From these examples, we can draw the following preliminary conclusions.

(1) The boundary flux updating technique has the potential to be used to determine reliable values of the basal HFD in hydrologically active areas. To model the interaction between the two regimes, both thermal and hydrological data are needed and should be inverted simultaneously.

(2) Lack of information on some physical quantities may be compensated by sufficient information on other physical quantities. This allows us to consider the sufficiency of information on the whole problem, instead of individual quantities, and introduces some practical flexibility. But, as is true for all inverse problems, the smaller the amount of *a priori* information available, the less successful is the solution; beyond a certain limit, no stable solutions can be obtained.

(3) In regions where the groundwater movement and heat flow are strongly coupled, such as the water recharge and discharge regions, the inverse solution is more sensitive to the noise in temperature and head data. More information, such as a few accurate temperature measurements, is needed in these sensitive regions if the inversion is to converge to reasonable solutions.

As a forward problem, equation system (7) and (8) is

non-linear in the field variables; as an inverse problem, it is non-linear in the material properties as well. The convergency of a Bayesian type inverse solution is also influenced by the quality of the *a priori* information (Jackson & Matsu'ura 1985). The *a posteriori* covariance matrix of a non-linear inverse problem given as a linear approximation does not always necessarily suggest the reliability of the estimates, and when the iteration converges to a wrong solution, the unreliability will not be fully revealed by the 1 s.d. uncertainty range (see Fig. 5(c) for example). This reflects the complexity of the *a posteriori* PDF of the parameters of a non-linear inverse problem; the solution may converge to a local maximum of the *a posteriori* PDF. Generally there is no way to be sure if a maximum is local or global; indeed the global maximum may not even be the best estimate point. With synthetic data, failure or success of the computation can be determined by comparing the solution with the true model, using a convenient criterion, such as whether the estimate is within 1 s.d. from the true value. Without a known true model, behaviour of the solution has to be judged intuitively. For example, there are two possibilities in evaluating the updated HFD in Fig. 6(c): (1) to accept the solution as a success, assuming that the oscillations in the HFD pattern are caused by an unknown process going on in the basement formation; (2) to reject the solution, on the basis that we know, somehow, that the basal HFD is unlikely to have short wavelength, large magnitude variations. If failure of the solution is suspected, more information should be sought or further assumptions invoked, to help constrain the solution. In one case we constrained the solution by using accurate temperature data from two hypothetical boreholes drilled in the discharge region; in another case, we constrained the solution by assuming spatial correlations in the basal HFD distribution.

When the problem is too poorly constrained, which often means insufficient data, the RTV scheme may not converge to any fixed point. In such a case, any Bayesian non-linear inverse method based on point estimates, as well as our particular iteration scheme, is invalid.

ACKNOWLEDGMENT

We acknowledge with thanks operating grants of the Natural Sciences and Engineering Research Council of Canada and Imperial Oil Limited; an Ontario Graduate Scholarship (KW); and helpful discussions and remarks from P. Y. Shen. We also thank L. Smith and A. Woodbury for critically reviewing the manuscript and making many valuable suggestions.

REFERENCES

Bachu, S., 1985. Influence of lithology and fluid flow on the temperature distribution in a sedimentary basin: a case study from the Cold Lake area, Alberta, Canada, *Tectonophysics*, **120**, 257–284.

Bathe, K. J. & Wilson, E. L., 1976. *Numerical Methods in Finite Element Analysis*, Prentice-Hall, Englewood Cliffs.

Bear, J., 1972. *Dynamics of Fluids in Porous Media*, American Elsevier, New York.

Beck, A. E. & Shen, P. Y., 1989. On a more rigorous approach to geoethermic problems, *Tectonophysics*, **164**, 1989.

Bejan, A., 1984. *Convection Heat Transfer*, Wiley, New York.

Bethke, C. M., 1985. A numerical model of compaction-driven groundwater flow and heat transfer and its application to the paleohydrology of intracratonic sedimentary basins, *J. geophys. Res.*, **90**, 6817–6828.

Box, G. E. P. & Tiao, G. C., 1973. *Bayesian Inference in Statistical Analysis*, Addison-Wesley, Reading, Massachusetts.

Carrera, J. & Neuman, S. P., 1986. Estimation of aquifer parameters under transient and steady state conditions: 2 Uniqueness, stability and solution algorithms. *Water Resour. Res.*, **22**, 211–227.

Čermak, V., 1989. Heat flow in a sedimentary basin in Czechoslovakia: evaluation of data with special attention to hydrology, in *Hydrological Regimes and Their Subsurface Thermal Effects*, eds Beck, A. E., Stegena, L. & Garven, G. Am. Geophys. Un. Monograph Series, Washington, 1989.

Čermak, V. & Jetel, J., 1985. Heat flow and ground water movement in the Bohemian Cretaceous Basin (Czechoslovakia), *J. Geodynamics*, **4**, 285–303.

Chapman, D. S., Keho, T. H., Bauer, M. S. & Picard, M. D., 1984. Heat flow in the Uinta Basin determined from bottom hole temperature (BHT) data, *Geophysics*, **49**, 453–466.

Cooley, R. L., 1977. A method of estimating parameters and assessing reliability for models of steady state groundwater flow: 2. Application of statistical analysis, *Water Resour. Res.*, **15**, 603–617.

Dagan, G., 1986. Statistical theory of ground water flow and transport: pore to laboratory, to formation and formation to regional scale, *Water Resour. Res.*, **22**, 120S-134S.

Freeze, R. A., 1975. A stochastic–conceptual analysis of one-dimensional ground water flow in nonuniform homogeneous media, *Water Resour. Res.*, **11**, 725–741.

Gavalas, G. R., Shah, P. C. & Seinfeld, J. H., 1976. Reservoir history matching by Bayesian estimation, *Soc. Petrol Eng. J.*, **16**, 337–350.

Gosnold, W. D. & Fischer, D. W., 1986. Heat flow studies in sedimentary basins, in *Thermal Modelling in Sedimentary Basins*, pp. 199–217, ed. Burrus, J. Technip, Paris.

Hitchon, B., 1984. Geothermal gradients, hydrodynamics, and hydrocarbon occurrences, Alberta, Canada, *Am. Assoc. Petrol Geol. Mem.* **66**, 713–743.

Hoeksema, R. J. & Kitanidis, P. K., 1984. An application of the geostatistical approach to the inverse problem in two-dimensional groundwater modeling, *Water Resour. Res.*, **20**, 1003–1020.

Hoeksema, R. J. & Kitanidis, P. K., 1985a. Analysis of the spatial structure of properties of selected aquifers, *Water Resour. Res.*, **21**, 563–572.

Hoeksema, R. J. & Kitanidis, P. K., 1985b. Comparison of Gaussian conditional mean and kriging estimation in the geostatistical solution of the inverse problem, *Water Resour. Res.*, **21**, 825–836.

Huyakorn, P. S. & Pinder, G. F., 1983. *Computational Methods in Subsurface Flow*, Academic Press, New York.

Jackson, D. D., 1979. The use of *a priori* data to resolve non-uniqueness in linear inversion, *Geophys. J. R. astr. Soc.*, **57**, 137–157.

Jackson, D. D. & Matsu'ura, M., 1985. A Bayesian approach to nonlinear inversion, *J. geophys. Res.*, **90**, 581–591.

Jones, F. W., Majorowitz, J. A. & Lam, H. L., 1985. The variation of heat flow density with depth in the Prairies Basin of western Canada, *Tectonophysics*, **121**, 35–44.

Kasameyer, P., L. Younker and J. Hanson, Inverse approach for thermal data from a convecting thermal system, *J. of Geodynamics*, **4**, 165–181, 1985.

Kitanidis, P. K. & Vomvoris, E. G., 1983. A geostatistical approach to the inverse problem in groundwater modeling (steady state) and one-dimensional simulations, *Water Resour. Res.*, **19**, 677–690.

Kuiper, L. K., 1986. A comparison of several methods for the solution of the inverse problem in two-dimensional steady state groundwater flow modeling, *Water Resour. Res.*, **22**, 705–714.

Luheshi, M. N. & Jackson, D., 1986. Conductive and convective heat transfer in sedimentary basins. in *Thermal Modelling in Sedimentary Basins*, pp. 219–234, ed. Burrus, J., Technip, Paris.

Majorowicz, J. A. & Jessop, A. M., 1981. Regional heat flow patterns in the Western Canadian sedimentary basin, *Tectonophysics*, **74**, 209–238.

Menke, W., 1984. *Geophysical Data Analysis: Discrete Inverse Theory*, Academic Press, Orlando.

Mercer, J. W., Pinder, G. F. & Donaldson, I. G., 1975. A Galerkin-finite element analysis of the hydrothermal system at Wairakei, New Zealand, *J. geophys. Res.*, **80**, 2608–2621.

Neuman, S. P. & Yakowitz, S., 1979. A statistical approach to the inverse problem of aquifer hydrology: 1. Theory, *Water Resour. Res.*, **15**, 845–860.

Nielsen, S. B., 1986. Continuous temperature log: theory and applications, *PhD thesis*, University of Western Ontario.

Neilsen, S. B., 1987. Steady state heat flow in a random medium and the linear heat flow–heat production relationship, *Geophys. Res. Lett.*, **14**, 318–321.

Rodgers, C. D., 1976. Retrieval of atmospheric temperature and composition from remote measurements of thermal radiation, *Rev. geophys. Space Phys.*, **14**, 609–624.

Schweppe, F. C., 1973. *Uncertain Dynamic Systems*, Prentice-Hall, New Jersey.

Shen, P. Y. & Beck, A. E., 1988. Inversion of temperature measurements in lake sediments, *Geophys. J. R. astr. Soc.*, **94**, 545–558.

Smith, L. & Chapman, D. S., 1983. On the thermal effects of groundwater flow: 1. Regional scale systems. *J. geophys. Res.*, **88**, 593–608.

Smith, L. & Freeze, R. A., 1979. Stochastic analysis of steady state groundwater flow in a bounded domain: 1. One-dimensional simulations, *Water Resour. Res.*, **15**, 521–528.

Sun, N. Z. & Yeh, W. W. G., 1985. Identification of parameter structure in groundwater inverse problem, *Water Resour. Res.*, **21**, 869–883.

Tarantola, A. & Valette, B., 1982. Generalized nonlinear inverse problems solved using the least squares criterion. *Rev. geophys. Space Phys.*, **20**, 219–232.

Vasseur, G., Lucazeau, F. & Bayer, R., 1986. The inverse problem of heat flow density determination from inaccurate data, *Tectonophysics*, **121**, 25–34.

Wang, J. Y., Wang, J. A., Xiong, L. P. & Zhang, J. M., 1985. Analysis of factors affecting heat flow density determination in the Liaohe Basin, North China, *Tectonophysics*, **121**, 63–78.

Wang, K. & Beck, A. E., 1987. Heat flow measurement in lacustrine or oceanic sediments without recording water bottom temperature variations, *J. geophys. Res*, **92**, 12837–12845.

Wang, K., Shen, P. Y. & Beck, A. E., 1989. A solution to the inverse problem of the coupled hydrological and thermal regimes, in *Hydrological Regimes and Their Subsurface Thermal Effects*, eds Beck, A. E., Stegena, L. & Garven, G., Am. Geophys. Un. Monograph Series, Washington, 1989.

Willett, S. D. & Chapman, D. S., 1987. On the use of thermal data to resolve and delineate hydrologic flow system in sedimentary basins: an example from the Uinta Basin, Utah, in *Proc. Third Canadian/American Conf. on Hydrology of Sedimentary Basins: Application to Exploration and Exploitation*, pp. 159–168, eds Hitchon, B., Bachu, S. & Sauveplace, C., National Water Assn., Dublin, Ohio.

Woodbury, A. D. & Smith, L., 1985. On the thermal effects of three-dimensional groundwater flow, *J. geophys. Res.*, **90**, 759–767.

Woodbury, A. D. & Smith, L., 1988. Simultaneous inversion of hydrogeologic and thermal data: 2. Incorporation of thermal data, *Water Resour. Res.*, **24**, 356–372.

Yeh, W. W-G. & Yoon, Y. S., 1981. Aquifer parameter identification with optimum dimension in parameterization, *Water Resour. Res.*, **17**, 664–672.

Zienkiewicz, O. C., 1972. *The Finite Element Method in Engineering Science*, McGraw-Hill, New York.

APPENDIX A: GRADIENT MATRIX

A direct differentiation of $\mathbf{g}(\mathbf{p})$ with respect to the components of $\mathbf{p}$ poses problems. However, according to (32), we have

$$\mathbf{g} = K \cdot U = \left(\sum_e K^e\right) \cdot U = \sum_e (K^e \cdot U) = \sum_e \mathbf{g}^e \tag{A1}$$

and hence

$$G_{lm} = \frac{\partial^i g_l}{\partial p_m} = \sum_e \frac{\partial^i g_l^e}{\partial p_m} = \sum G_{lm}^e. \tag{A2}$$

Since the differentiation is of the first order, the placement of the left superscript i of g right after ∂ should not create any confusion. The same comments apply to the following derivations.

Therefore, the G matrix can be derived for individual elements and assembled at the global level. The entries of the elemental G matrix are derived as follows, with λ and κ assumed to be isotropic,

$$\frac{\partial^1 g_l^e}{\partial T_m} = {}^{11}K_{lm}^e + \frac{\partial^{11} K_{lk}^e}{\partial T_m} T_k = {}^{11}K_{lm}^e - \int_{\Omega^e} \rho c \kappa H_l H_m (\eta v_i' - \beta g \mu^{-1} \delta_{2i}) \frac{\partial H_k}{\partial x_i} d\Omega\, T_k, \tag{A3}$$

where $v_i' = \rho_0 g[(\partial H_n/\partial x_i)h_n + \rho_r \delta_{2i}]$

$$\mu^{-1} = \mu_0^{-1} + \eta(H_n T_n - T_0)$$

$$\frac{\partial^1 g_l^e}{\partial h_m} = \frac{\partial^{11} K_{lk}^e}{\partial h_m} T_k = -\int_{\Omega^e} \rho c \mu^{-1} \kappa \rho_0 g H_l \frac{\partial H_m}{\partial x_i} \frac{\partial H_k}{\partial x_i} d\Omega\, T_k \tag{A4}$$

$$\frac{\partial^1 g_l^e}{\partial \gamma} = \frac{\partial^{11} K_{lk}^e}{\partial \gamma} T_k = \int_{\Omega^e} \lambda \frac{\partial H_l}{\partial x_i} \frac{\partial H_k}{\partial x_i} d\Omega\, T_k \tag{A5}$$

$$\frac{\partial^1 g_l^e}{\partial \psi} = \frac{\partial^{11} K_{lk}^e}{\partial \psi} T_k = -\int_{\Omega^e} \rho c \kappa \mu^{-1} v_i' H_l \frac{\partial H_k}{\partial x_i} d\Omega\, T_k \tag{A6}$$

$$\frac{\partial^2 g_l^e}{\partial T_m} = {}^{21}K_{lk}^e + \frac{\partial^{21} K_{lk}^e}{\partial T_m} T_k + \frac{\partial^{22} K_{lk}^e}{\partial T_m} h_k = {}^{21}K_{lm}^e - \int_{\Omega^e} \kappa g\, \delta_{2i} \eta \beta H_m \frac{\partial H_l}{\partial x_i} H_k\, d\Omega\, T_k + \int_{\Omega^e} \kappa \eta \rho_0 g H_m \frac{\partial H_l}{\partial x_i} \frac{\partial H_k}{\partial x_i} d\Omega\, h_k \tag{A7}$$

$$\frac{\partial^2 g_l^e}{\partial h_m} = {}^{22}K_{lm}^e \tag{A8}$$

$$\frac{\partial^2 g_l^e}{\partial \gamma} = 0 \tag{A9}$$

$$\frac{\partial^2 g_l^e}{\partial \psi} = {}^{21}K_{lm}^e T_k + {}^{22}K_{lm}^e h_k = {}^{2}g_l^e. \tag{A10}$$

APPENDIX B: COVARIANCE MATRIX $\hat{C}_{qq}$

Denoting $G \cdot C_{pp} \cdot G^t$ by R', and substituting (4) into (6), we have,

$$\begin{aligned}
\hat{C}_{ff} &= R' - R' \cdot (R' + C_{ff})^{-1} \cdot R' \\
&= R' - R' \cdot (R' + C_{ff})^{-1} \cdot (R' + C_{ff} - C_{ff}) \\
&= R' - R' \cdot [I - (R' + C_{ff})^{-1} \cdot C_{ff}] \\
&= R' \cdot (R' + C_{ff})^{-1} \cdot C_{ff} \\
&= (R' + C_{ff} - C_{ff}) \cdot (R' + C_{ff})^{-1} \cdot C_{ff} \\
&= C_{ff} - C_{ff} \cdot (R' + C_{ff})^{-1} \cdot C_{ff}.
\end{aligned} \tag{B1}$$

Using (48) after substituting (44) into equation (B1), we obtain the simple form of $\hat{C}_{qq}$ as given by (50).